Drying Process Paths of Ternary Polymer Solution Coating

Mahendra Dabral, L. F. Francis, and L. E. Scriven
Dept. of Chemical Engineering & Materials Science and Center of Interfacial Engineering,
University of Minnesota, Minneapolis, MN 55455

Drying process paths of a ternary solution consisting of a polymer dissolved in a blend of a solvent and a nonsolvent are analyzed. A 1-D drying model applied to a ternary solution provides composition trajectories followed at different depths in the coating as a function of time, collectively called process paths. The effects of gas-phase mass-transfer coefficient, relative diffusivity and relative volatility, and partial saturation of the gas phase with solvents on these process paths are presented. When the solution coating enters the two-phase region, phase separation may take place, as illustrated by coatings prepared from ternary solutions of cellulose acetate in ketone and methanol. When acetone is the solvent, the coating phase separates. Replacing acetone with methyl ethyl ketone gives homogeneous coatings. Solution phase separation or "blush" is explained in terms of the drying-process paths and their relationship to the two-phase immiscible region.

Introduction

Mixtures or blends of solvents are commonly employed in coating formulations. The reasons range from solubilizing one or more polymeric constituents, to controlling the rate of drying as the solvents depart, to achieving surface tension vs. relative volatility that is favorable to leveling and defect suppression, to lowering cost by replacing some of an expensive, well-suited solvent by a cheaper, less well-suited one. The art of choosing solvents to blend in a coating formulation is based on the standard aspects of the solubility behavior of the solvents and the polymers involved. These aspects are codified in correlations of the solubility parameters, as to which phase behavior can be related. The most useful relation is through the Flory-Huggins model of the behavior of polymer solutions, as employed below.

In the drying of some coating formulations the goal is to maintain the polymer–solvent solution as a single phase until it gels and/or vitrifies to solidify the coating, as in the case of solvent-cast cellulose triacetate coatings (Tsujimoto, 1998). In contrast, in the drying of certain asymmetric porous polymeric membranes, which are cast as coatings on a substrate and then are stripped to become freestanding, the goal is to induce during drying a graded phase separation with depth into the coating (Koros and Pinnau, 1994; Shojaie et al., 1994a; Kesting, 1985; Mulder, 1991). The resulting pore-size gradient is the outcome of rate competition between the diffusion and evaporation of volatile solvents on the one hand, and supersaturation and phase separation by nucleation and growth or spinodal decomposition on the other hand. The rate competition and final microstructure are controlled by the choice of solvents, temperature, partial pressures of solvents in the adjoining vapor phase, and the mass-transfer coefficient there (Dabral, 1999). In the drying of certain reactive coating solutions, the solvent blend can be designed to hold products as well as reactants in solution until the coating gels and/or vitrifies, but thereafter to allow the remaining solvent to be removed by drying. In the drying of certain thick (500 μm) coatings of colloidal particulates in binder solution, a lower volatility solvent is added to avoid premature dryout, shrinkage stress, and "mudcracking" of the surface zone (Sullivan, personal communication, 1994). Many other examples of the use of mixed solvents could be adduced.

This article puts forward the concept of process paths as a tool for analyzing and understanding the drying of polymeric coatings containing two volatile solvents that form a single solution phase with polymer as coated. The process paths in a drying coating are the entire family of trajectories of com-

Correspondence concerning this article should be addressed to L. F. Francis.

position vs. time, at all relative depths in the coating. By relative depth, we mean the depth of a given stratum of polymer as a fraction of the current total depth of the coating. The total depth, of course, diminishes with time, as solvent evaporates from the coating's free surface. More precisely, a process path is here defined as the composition trajectory at a fixed polymer material coordinate; because it is not volatile, the polymer must remain in the coating.

The process-path concept is developed and illustrated by means of a well-established theory of one-dimensional mass and heat transfer in transversely uniform coating (Okazaki et al., 1974; Cairncross et al., 1992; Vrentas and Vrentas, 1994; Shojaie et al., 1994b). In a transversely uniform coating, composition and temperature vary solely in depth, the one dimension. The resulting sets of equations that quantify the composition of the volatiles in the thin liquid coating are essentially the same as the mass-transfer analysis of asymmetric membrane formation by immersion of a polymer solution into a nonsolvent bath (Reuvers et al., 1987; Tsay and McHugh, 1990; Cheng et al., 1994); the asymmetric porous structure of these membranes was predicted by superposing the calculated mass-transfer path of the entire coating on the two-phase region. Adachi and Scriven (1992) quantified plasticizer migration by calculating the mass-transfer paths of the top and bottom of a liquid coating in a polymer, solvent, and nonvolatile plasticizer system. Shojaie et al. (1994b) also calculated the mass-transfer path of the top and bottom of a drying liquid coating of a cellulose acetate, water, and acetone ternary system. They used these calculations to predict the effect of film thickness and initial concentration on the final structure of the porous membranes. In all of these prior reports, a systematic evolution of mass-transfer paths as a function of depth, and their dependence on drying process parameters, is absent. In this work, we report calculations of process paths and progress along them and how they depend on the relative diffusivities ("speeds") of the two solvents, on their relative volatilities ("low boiling" vs. "high boiling"), on the gas-phase mass-transfer coefficient ("intensity of drying"), and on the partial pressures of the solvents in the adjoining phase ("gas saturation control").

Process paths become a powerful tool when they are plotted on the equilibrium ternary-phase diagram of the two solvents and polymer (plus temperature when the process departs significantly from isothermal), and that diagram contains one or more multiphase regions, that is, ranges of composition that at equilibrium separate into two (or even three) coexisting phases (the condition of "incompatibility"). As shown here, the process paths then illuminate whether a given formulation is likely to suffer phase separation ("blushing," "haze," and so on) during drying. This is further illustrated by coatings prepared from ternary solutions of cellulose acetate in acetone and methanol, where the solution coating enters the two-phase region. The resulting "blush" or phase separation is similar to the precipitation induced by nonsolvent invasion from a bath into a binary polymer solution coating; the latter technique is used to prepare porous asymmetric membranes (Tsay and McHugh, 1990). Process paths acquire even greater utility when a gelation or vitrification boundary can be located on the equilibrium diagram, as it often can be (Strathmann et al., 1971; Radovanovic et al., 1992; Dabral, 1999).

The drying process path analysis of this work is aimed at providing a valuable tool in dryer design, solvent selection, process manipulation, and defect elimination in coatings that contain multiple solvents. What follows is divided into three sections. The first summarizes the equations of change of component masses, the boundary conditions, the chosen constitutive equations of solution behavior and diffusion, and the means of computing predictions from those inputs. The second section compares illustrative predictions of the theory for different boundary conditions and constitutive behavior. The third section covers the predictions of phase behavior and process paths of drying cellulose acetate/ketone/methanol coatings along with experimental observations of coatings that dry faster because they contain acetone, with those that dry slower because they contain methyl ethyl ketone instead.

Theory

In the ternary system, for convenience, the better solvent is called the solvent and the poorer one is called the nonsolvent. In what follows the solvent and polymer are miscible in all proportions; the nonsolvent and polymer are not (they have a range of "incompatibility"). Figure 1 shows the drying of a thin solution coating atop an impermeable substrate. By hypothesis the composition varies only in the z-direction. Table 1 lists the equations of change of component molar densities; it also records the boundary conditions and formulas for equilibrium partial pressures according to the Flory-Huggins constitutive relation of ternary polymer solutions (Flory, 1953). The phase diagram below is from the same constitutive relation.

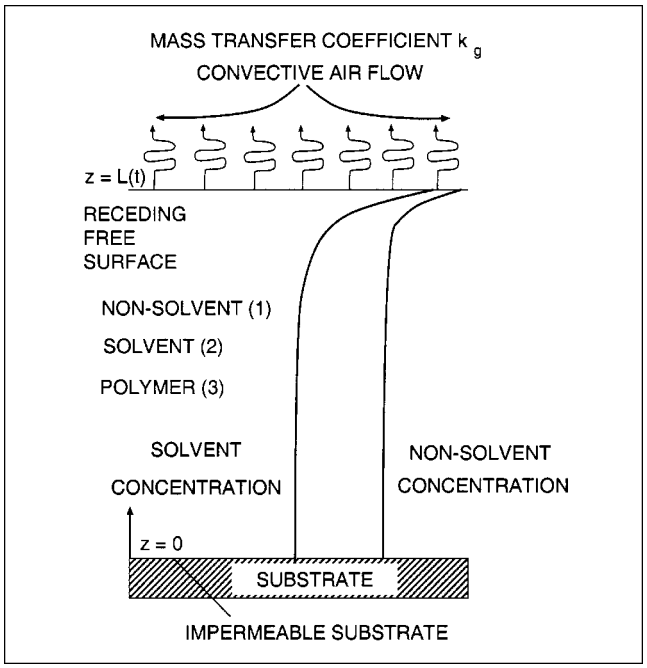

Figure 1. One-dimensional drying of a ternary polymer solution coating.

Table 1. Mass-Balance Equations for Drying of Ternary Polymer Solution Coating

Description	Equation
Mass balance of solvent (species 1)	$\frac{\partial c_1}{\partial t} = \frac{\partial}{\partial z}\left(D_{11}\frac{\partial c_1}{\partial z}\right) + \frac{\partial}{\partial z}\left(D_{12}\frac{\partial c_2}{\partial z}\right)$
Mass balance of nonsolvent (species 2)	$\frac{\partial c_2}{\partial t} = \frac{\partial}{\partial z}\left(D_{22}\frac{\partial c_2}{\partial z}\right) + \frac{\partial}{\partial z}\left(D_{21}\frac{\partial c_1}{\partial z}\right)$
Boundary condition, flux of solvent (1) at the free surface	$\left(-D_{11}\frac{\partial c_1}{\partial z} - D_{12}\frac{\partial c_2}{\partial z}\right)\Big\|_{z=L(t)} = (1-c_1\overline{V}_i)k_g(p_{1i}^G - p_{1b}^G) - c_1\overline{V}_2 k_g(p_{2i}^G - p_{2b}^G)$
Boundary condition, flux of nonsolvent (2) at the free surface	$\left(-D_{22}\frac{\partial c_2}{\partial z} - D_{21}\frac{\partial c_1}{\partial z}\right)\Big\|_{z=L(t)} = (1-c_2\overline{V}_2)k_g(p_{2i}^G - p_{2b}^G) - c_2\overline{V}_1 k_g(p_{1i}^G - p_{1b}^G)$
Boundary condition, flux of solvent (1) at the base	$\left(-D_{11}\frac{\partial c_1}{\partial z} - D_{12}\frac{\partial c_2}{\partial z}\right)\Big\|_{z=0} = 0$
Boundary condition, flux of nonsolvent (2) at the base	$\left(-D_{22}\frac{\partial c_2}{\partial z} - D_{21}\frac{\partial c_1}{\partial z}\right)\Big\|_{z=0} = 0$
Film thickness, overall mass balance	$\frac{dL}{dt} = \overline{V}_1 k_g(p_{1i}^G - p_{1b}^G) - \overline{V}_2 k_g(p_{2i}^G - p_{2b}^G)$
Equilibrium solvent partial pressure (1)	$\ln\left(\frac{p_{1i}}{p_1^{vap}(T)}\right) = \ln\phi_1 + \left(1-\frac{1}{n}\right)\phi_3 + \chi_{13}\phi_3^2 + \chi_{12}\phi_2^2 + \phi_2\phi_3(\chi_{13} + \chi_{12} - \chi_{23})$
Equilibrium nonsolvent partial pressure (2)	$\ln\left(\frac{p_{2i}}{p_2^{vap}(T)}\right) = \ln\phi_2 + \left(1-\frac{1}{n}\right)\phi_3 + \chi_{23}\phi_3^2 + \chi_{12}\phi_1^2 + \phi_1\phi_3(\chi_{12} + \chi_{23} - \chi_{13})$

Process-path analysis

In this section, the mass- and energy-balance equations of a drying solution coating are solved to obtain compositions as a function of time and depth in the coating. These calculations demonstrate the dependence of process paths on the relative volatility and relative diffusivity of solvents, and on external drying conditions, namely mass flow rate and partial pressures of solvents in the gas phase. The results presented here depend on a few simplifications that have been made in the calculations, and these are now described.

The equations of change of solvent and nonsolvent molar densities, listed in Table 1, include the cross-term ternary diffusion coefficients. Multicomponent diffusion effects in polymer–solvent systems can lead to large cross-term diffusion coefficients; however, because of a lack of reliable experimental data and the absence of a suitable predictive theory, these cross-term diffusion coefficients, D_{12} and D_{21}, are set to zero in this work. Theoretical descriptions of ternary diffusion that take into account the cross-term diffusion coefficients have been proposed (Reuvers et al., 1987). However, these complicated models also rely on various simplifications [for example, that the ternary frictional coefficients have a certain concentration dependence so that they can be related to binary frictional coefficients, and the frictional coefficient between the polymer and solvent has a certain character (Reuvers et al., 1987; Tsay and McHugh, 1990; Shojaie et al., 1994b)]. If necessary, the calculations presented in this work can readily be augmented to incorporate these concentration-dependent cross-term diffusion coefficients. The main-term diffusion coefficients, D_{11} and D_{22}, are set as exponential functions of polymer volume fraction. This strong dependence of solvent diffusivity on polymer concentration is a characteristic of polymer–solvent systems (Vrentas and Duda, 1987). The solvent and nonsolvent main-term diffusion coefficients are thus $D_{11} = D_{10}\exp(-\beta_{NS}\phi_p)$ and $D_{22} = D_{20}\exp(-\beta_S\phi_p)$, where ϕ_p is the polymer volume fraction. D_{10} and D_{20} are the diffusion coefficients of nonsolvent and solvent in the zero polymer concentration limit, and are set equal. Consequently, the exponent β determines how strongly the diffusivity depends on polymer concentration. Figure 2 shows that a higher value of β gives a lower diffusion coeffi-

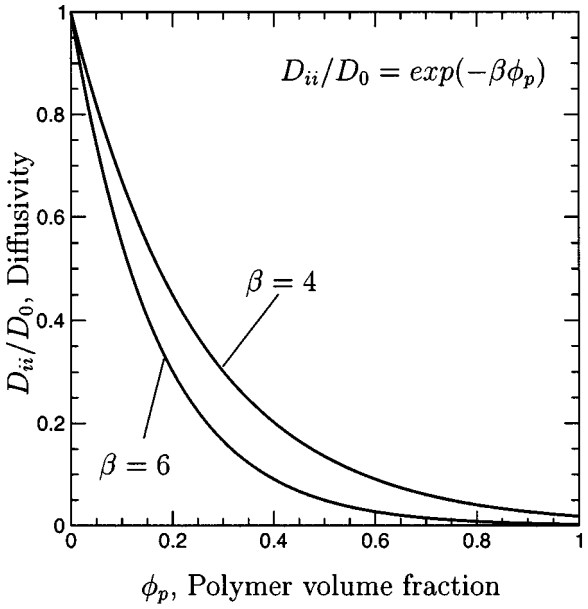

Figure 2. Exponential dependence of solvent and nonsolvent diffusivity on polymer concentration.

Table 2. Dimensionless Variables and Parameters in Mass-Balance Formulation of a Drying Coating

Variables	Dimensionless
Dimensionless time, τ	$\frac{D_0 t}{L_0^2}$
Relative depth in coating, η	$\frac{z}{L(t)}$
Nonsolvent Biot no., Bi_m^1	$\frac{\overline{V}_1 p_1^{\text{vap}}(T) k_g L_0}{D_0}$
Solvent Biot no., Bi_m^2	$\frac{\overline{V}_2 p_2^{\text{vap}}(T) k_g L_0}{D_0}$
Nonsolvent relative volatility, α	$\frac{p_1^{\text{vap}}(T)}{p_2^{\text{vap}}(T)}$
Nonsolvent gas-phase conc., c_{eq}^1	$\frac{p_{1b}^G}{\alpha_1 p_1^{\text{vap}}(T)}$
Solvent gas-phase conc., c_{eq}^2	$\frac{p_{2b}^G}{\alpha_1 p_2^{\text{vap}}(T)}$

cient over the entire concentration range. Moreover, the solvent diffusivity in the pure polymer limit is lower when β is smaller.

In order to illustrate simply the effects of solvent relative volatility and diffusivity, drying is taken to be isothermal. In reality, the evaporative cooling that accompanies rapid evaporation often produces temporary cooling at the start of drying, and the temperature of the coating is often raised by stages during drying. These complications are not considered here. This simplification is reasonable when heat-transfer coefficients are high.

The key dimensionless parameters of the ternary-solution drying model are summarized in Table 2. The mass Biot number of nonsolvent and solvent quantify the competition between rates of internal and external mass transfer. Here the partial molar volumes of the solvents are taken to be equal, that is, $\overline{V} = \overline{V}_2$. The mass Biot numbers of solvent and nonsolvent then relate to each other by

$$\frac{Bi_m^1}{Bi_m^2} = \frac{p_1^{\text{vap}}(T)}{p_2^{\text{vap}}(T)} \equiv \alpha, \tag{1}$$

where α is the relative volatility, that is, the ratio of pure nonsolvent vapor pressure to solvent vapor pressure, at the given temperature. The other two key drying process parameters are the gas-phase partial pressures, p_{1b}^G and p_{2b}^G, of solvent and nonsolvent. These parameters are quantified by the dimensionless gas-phase compositions c_{eq}^1 and c_{eq}^2, which are defined in Table 2.

In the next section, drying process paths are computed for different sets of process parameters. These computed solvent and nonsolvent concentrations are then plotted on a ternary composition diagram. Additionally, the phase behavior of the ternary polymer solution is also plotted on the diagrams. The phase behavior is described with the Flory-Huggins thermodynamics of ternary polymer solutions; the thermodynamic interaction parameters were set as $\chi_{12} = \chi_{13} = 1$ and $\chi_{23} = 0$. This simplified set of parameters describes the essential features of a ternary polymer, solvent, and nonsolvent system. However, the phase behavior can be readily computed for systems where the Flory-Huggins's interaction parameters are concentration dependent (Yilmaz and McHugh, 1986). In cases where the process paths invade the two-phase region in the ternary composition diagram, the drying model of a homogeneous liquid coating is no longer valid. However, the process path that those calculations lead to is useful for estimating at what depth and at what time the coating enters the two-phase region.

Path analysis and drying conditions

When the coating is sufficiently thin and/or the diffusion and convection of solvents into the gas phase are sufficiently slow, drying is controlled by the external resistance to mass transfer, that is, the Biot number is much less than unity. Then, the solvent concentrations vary negligibly with depth in the coating, and the family of paths collapses into a single path. This is illustrated in Figure 3a, which is for $Bi_m^1 = 0.1$ and $Bi_m^2 = 0.5$. As it departs from the initial composition (0.7 vol. fract.: S; 0.2 vol. fract.: NS), the path in Figure 3a heads away from the solvent vertex, since in this illustration the solvent partial pressure is initially five times that of the nonsolvent. However, after later approaching close to the binodal boundary of the two-phase region, the path veers away from the nonsolvent vertex as well, because even though the solvent has higher vapor pressure, its partial pressure at the surface is slight after most of it has departed from the coating. The figure also shows the dimensionless time along the drying paths, which are virtually one. The nonsolvent is the last to leave, as reflected by the path's approach along the base of the triangle to the polymer vertex. If the relative volatilities are reversed, from 0.2 to 5, the initial solvent partial pressure is only 0.2 times that of the nonsolvent, and the path initially heads away from the nonsolvent vertex, as shown in Figure 3b. The nonsolvent mass Biot number is 0.1 and that of the solvent is 0.02. Most of the nonsolvent departs before even half of the solvent. The path approaches the polymer vertex very close to the solvent–polymer side of the triangle; the solvent is last to leave. The drying takes much longer in Figure 3b because of the lower solvent mass Biot number of 0.02 compared to 0.5 in Figure 3a. In Figure 3 the diffusivities of solvent and nonsolvent are identical in magnitude and depend on their total volume fraction, as shown in Figure 2.

When the coating is 100 times thicker than that in Figure 3, or the convective diffusion of the solvents in the gas is 100 times faster, or some equivalent combination, drying is controlled by the internal resistance, that is, the Biot number is 10, greatly in excess of unity. This is illustrated in Figure 4a, which is for comparison with Figure 3a. Now the coating's surface dries faster than its base, and the family of paths fans out. The path of the surface in Figure 4a resembles the path in Figure 3a, but does not closely approach the two-phase region. The reason is that the diffusional resistance of the coating prevents the solvent concentration at the surface from falling as low as in Figure 3a, while the nonsolvent concentration is still fairly high there. The deeper into the coating the path is, the less it is affected by the relative volatility of solvent and nonsolvent at the surface.

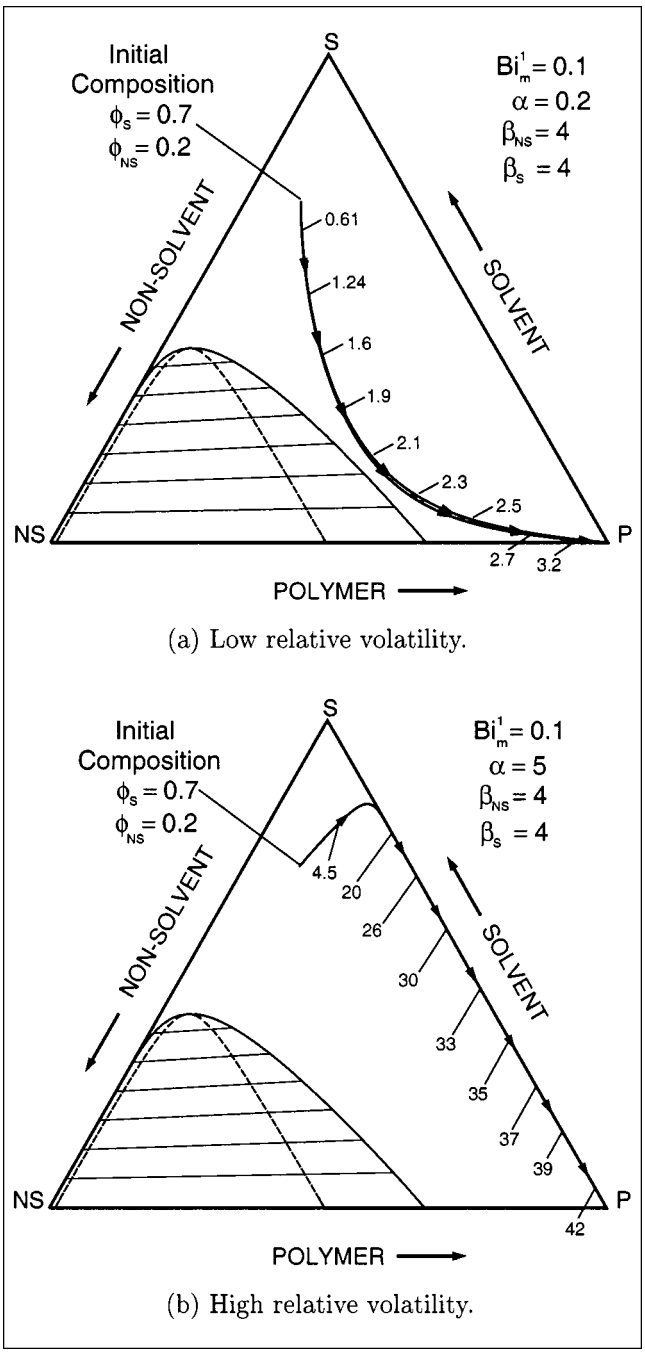

Figure 3. Process paths for $Bi_m = 0.1$.

Dimensionless times given along process paths.

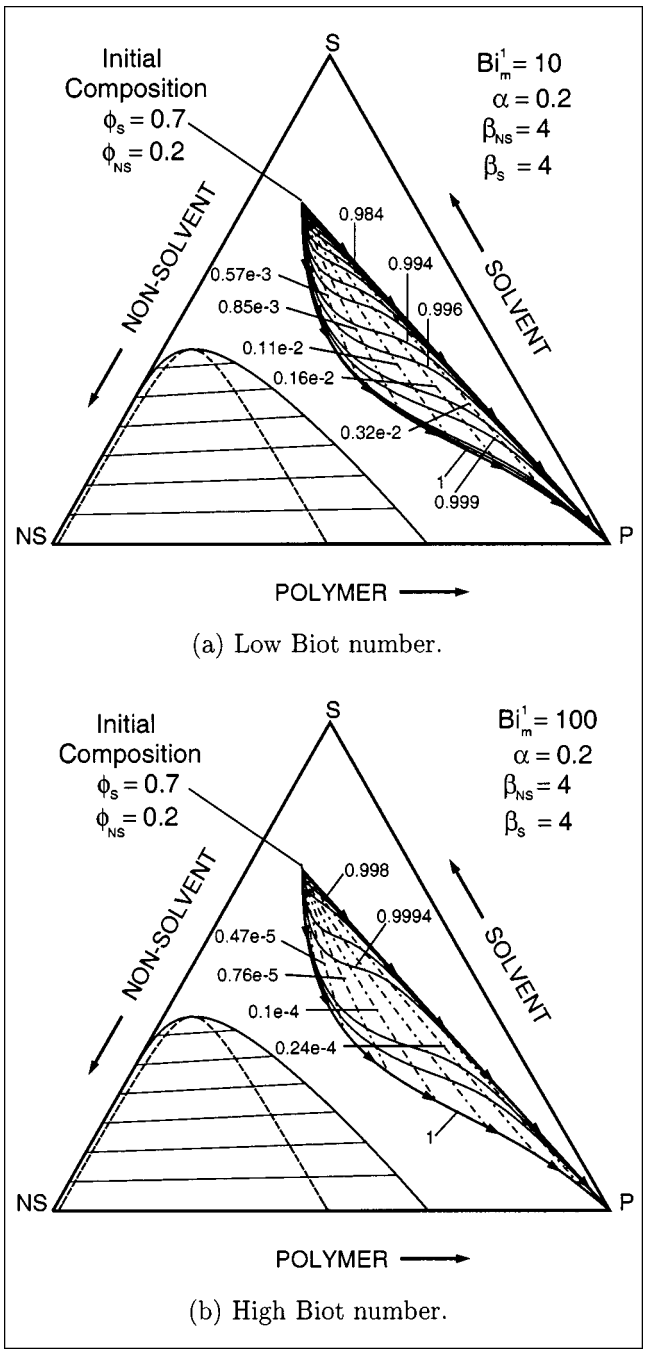

Figure 4. Process paths for $Bi_m = 10$ and $Bi_m = 100$.

Dashed lines show instantaneous concentration profiles at dimensionless times indicated. Solid lines are paths at different relative positions.

Indeed, the bulk of the coating in Figure 4a follows a path that is almost straight from the initial composition to the polymer vertex: the ratio of volume fractions of the two volatile species is virtually constant along this path. The reason is that starting early in the process, efflux from that depth is almost totally controlled by the diffusivities of the solvent and nonsolvent, which in this illustration are equal (regardless of the relative proportions of the two). Early in the process the coating surface comes close to equilibrium with the gas phase, which in this illustration is devoid of solvents. Thereafter, the very low surface concentrations of solvents changed little compared with change at the base of the coating. Both solvents there diffuse as though toward an almost totally solvent-free surface and, because they have the same diffusivity, do so at exactly the same rate. Later in this section it is described when the solvents have different diffusivities.

Along the family of paths, the rate of change of composition can be indicated by marking selected isochronal points,

as in Figure 4. A set of these points, of course, constitutes an instantaneous composition profile, that is, composition vs. relative depth in the drying, and therefore thinning coating. Such profiles at the indicated dimensionless times are marked by dot-dash curves in Figure 4 *et seq*. Also, the composition paths at the indicated dimensionless relative depths are marked by solid lines in Figure 4 *et seq*.

When the coating is so thick, or the convective diffusion action in the gas so intense, that the Biot number exceeds 10, the process paths and instantaneous composition profiles, except in the earliest moments, are indistinguishable from those at $Bi_m^1 = 10$ in Figure 4a—or from those as $Bi_m^1 \to \infty$ (not shown). In other words, the external resistance to mass transfer is negligible except as the coating first starts to dry. Although predictions could have been calculated for the limiting case as $Bi_m^1 \to \infty$, it was more convenient to choose $Bi_m^1 = 10$ for the cases compared here.

The process paths in Figures 4a and 4b show that the bulk of the coating $0 < \eta < 0.95$ follows the same path as the base of the coating. At high Biot numbers, the surface dries rapidly, and the bulk of the solvent loss is by diffusion of volatiles through the coating. The volatiles at the surface of the coating ($\eta = 1$) depart at increasingly shorter times as the mass Biot number is raised. In contrast, at high mass Biot numbers the volatiles at the base depart at the same rate, independent of the mass Biot number.

At intermediate Biot numbers, the internal and external resistances to mass transfer are comparable. Consequently, the process paths followed by the near-surface region and near-base region depend on both relative diffusivity and volatility of the solvents. Figure 5a shows the drying process paths for Biot number 0.5; the path followed by the base is no longer a straight line as it was in Figures 4a and 4b. Clearly, solvent loss at the base does not depend entirely on the diffusivities of solvents, as in the case of Figure 4. Figure 5b shows process paths for the case of $Bi_m^1 = 1$. However, these do not differ appreciably from those of Figure 4 because the solvent Biot number, Bi_2^m, is 5, which is high enough for internal resistance to dominate the drying process.

The process paths in the near-base region of a drying coating depend on the relative diffusivity of the volatiles. Figure 6 shows process paths of a drying coating where the solvent and nonsolvent diffuse at different rates. The paths followed by the near-surface region are independent of relative diffusivities at Biot numbers exceeding 10. When the nonsolvent has a higher diffusivity, as in Figure 6a, the nonsolvent depletes at a higher rate and the process paths near the base head toward the polymer–solvent axis. In contrast, when the solvent has a higher diffusivity, as in the case of Figure 6b, the solvent depletes at a relatively higher rate than the nonsolvent, and the process paths near the base bend away from the polymer–solvent axis.

When a solution coating contains enough nonsolvent that the initial composition lies close to the thermodynamically unstable regions, there is a possibility that the process paths may invade the two-phase region and even cause phase separation. Such an example is shown in Figure 7a, where the paths followed by the near-surface region enter the thermodynamically unstable region. In this case the solvent has greater volatility than the nonsolvent. If solvent diffusivity also exceeds that of the nonsolvent, then the near-base region of the coating also enters the two-phase region. However, this can be avoided by replacing the solvent with one that has a lower volatility and diffusivity. Figure 7b shows how this choice can cause the entire set of process paths to veer away from the two-phase region.

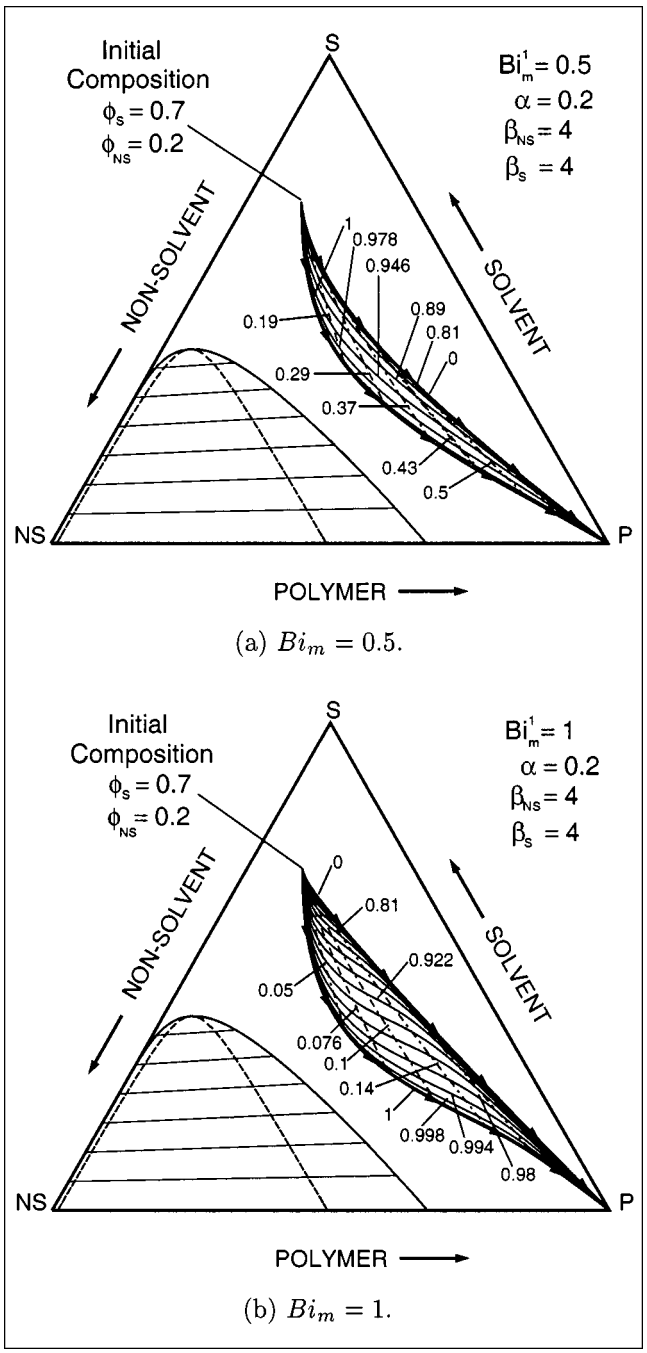

Figure 5. Process paths at intermediate Biot numbers.

Another way of controlling the solvent and nonsolvent flux in a drying coating is by partially saturating the gas phase with solvent and nonsolvent vapors. This reduces the driving force of mass transfer in the gas phase and alters the drying process paths. Figure 8a shows an example of a drying coat-

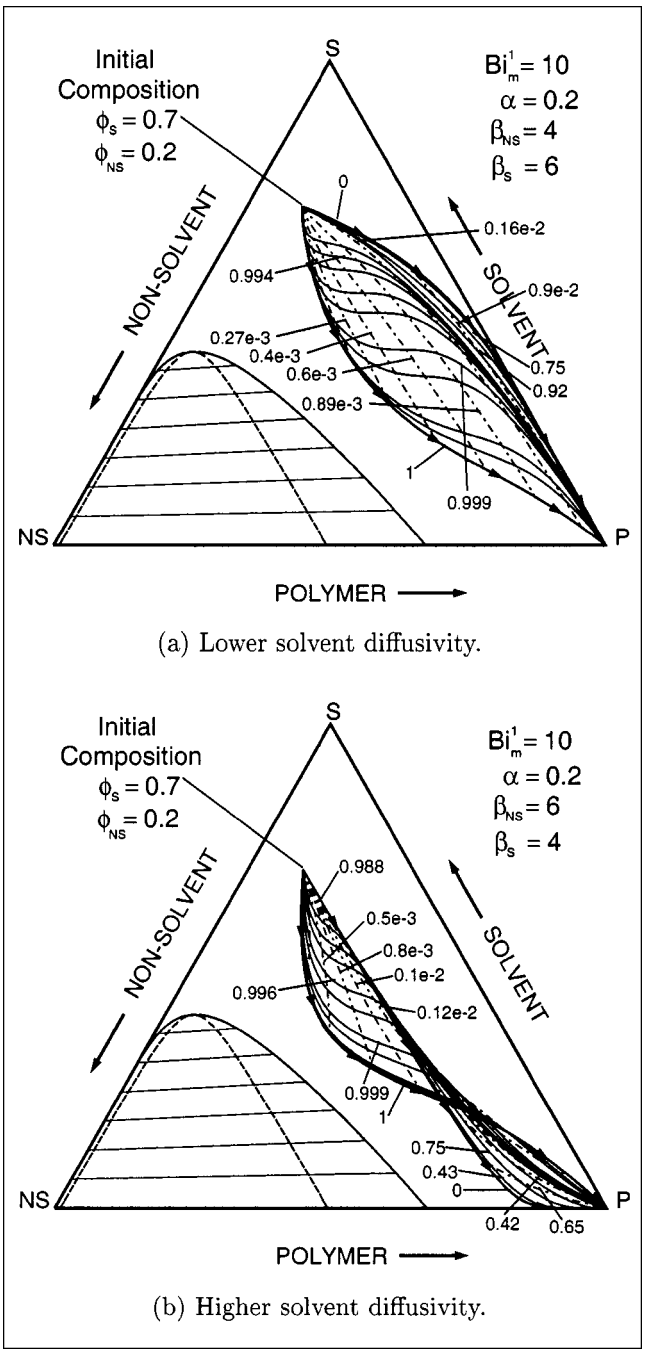

(a) Lower solvent diffusivity.

(b) Higher solvent diffusivity.

Figure 6. Process paths and effect of relative diffusivity.

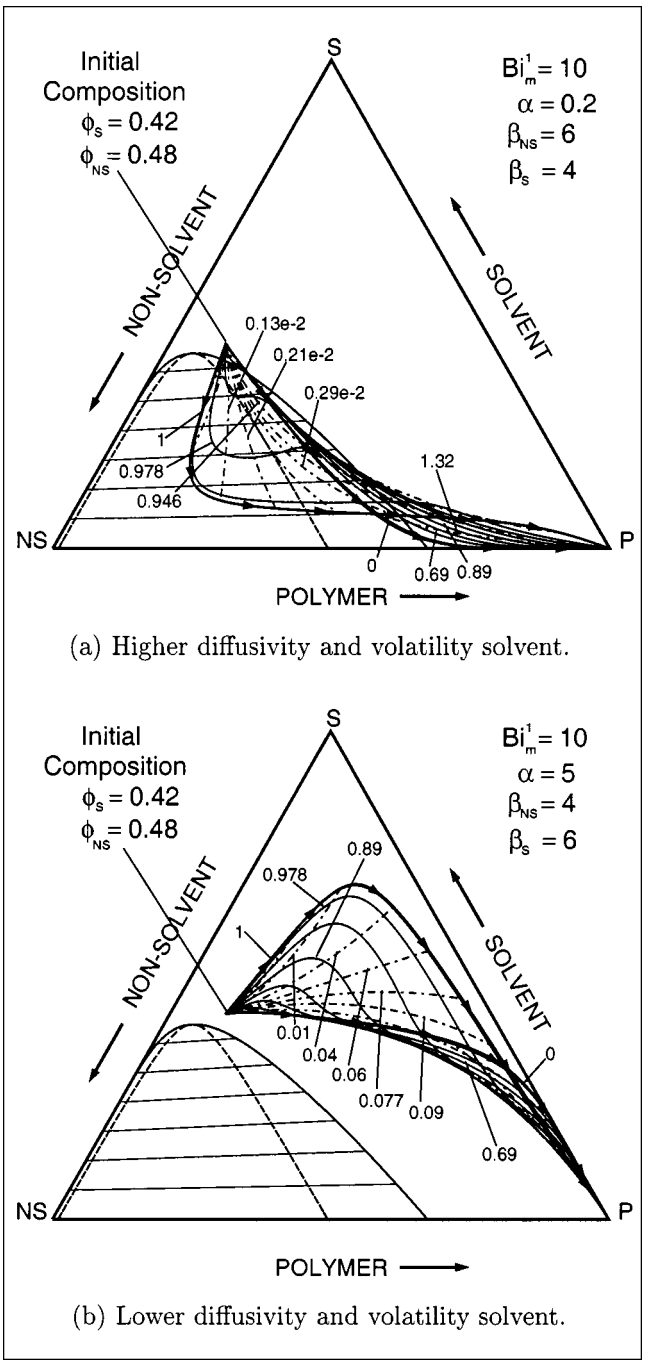

(a) Higher diffusivity and volatility solvent.

(b) Lower diffusivity and volatility solvent.

Figure 7. Effect of solvent volatility and diffusivity on process paths.

ing where the process paths of the near-surface region invade the binodal, which may lead to phase separation. Figure 8b shows the process paths of the same coating when it is dried with a solvent-enriched gas phase. The drying in Figure 8b is accomplished in two stages. In the first stage, $\tau < 0.5$, the gas-phase composition is set as $c_{eq}^1 = 0.6$, $c_{eq}^2 = 0$. The solvent vapors in the gas phase reduce the solvent's flux relative to the nonsolvent's and cause the process paths to veer away from the two-phase region. To complete the drying, the coating is dried in the second stage with a gas devoid of solvents, that is, $c_{eq}^1 = c_{eq}^2 = 0$ as shown in Figure 8b.

With the results of the theoretical modeling in our article, it is possible rationally to adjust formulation and process—even to design them—where the phase separation is to be selectively induced along the thickness direction. For example, as brought out in the text, a solvent with a higher volatility and lower diffusivity than the nonsolvent would cause the near-surface region of the coating to traverse the

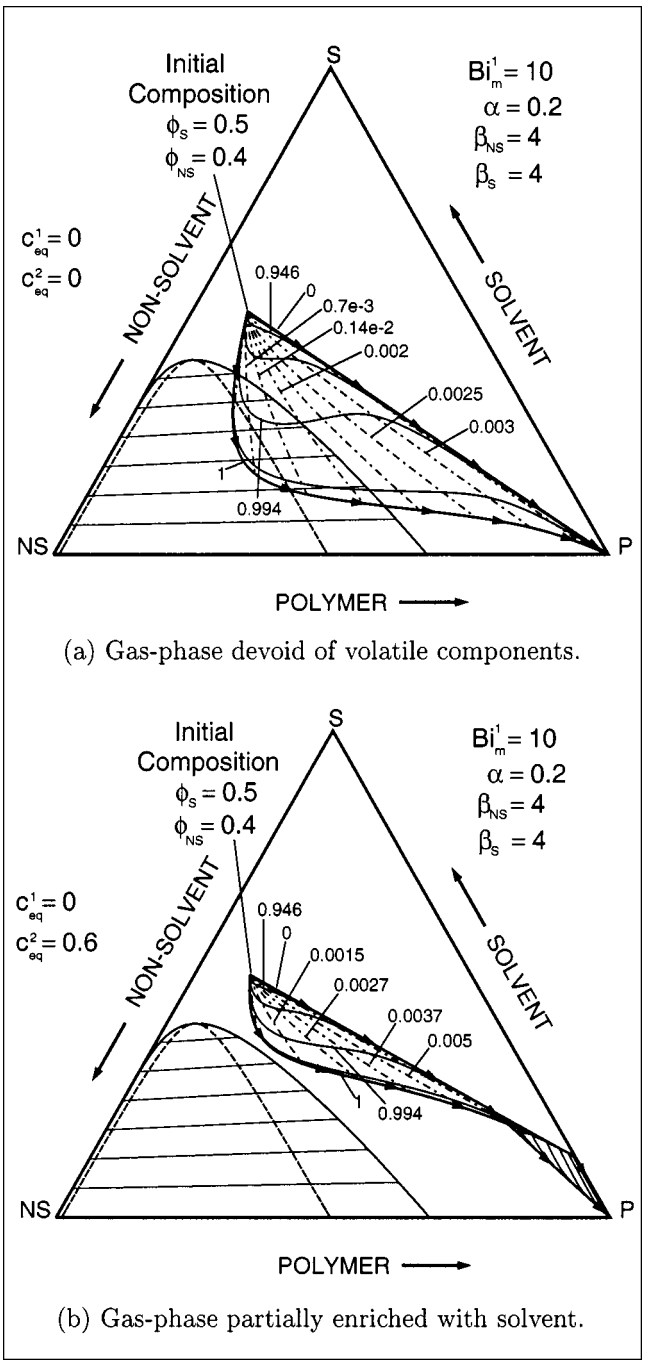

Figure 8. Avoiding phase separation by using solvent-enriched gas phase.

two-phase region. If the solvent volatility were successively reduced (say by choosing different solvents of the same type), then the thickness of the region where phase separation takes place would be reduced. In the next section, we provide a similar example of "blushing" or phase separation, and its dependence on the choice of solvent in a drying coating.

"Blush" or Phase Separation

The results in the previous section demonstrate that solution coatings consisting of multiple solvents can enter regions of immiscibility and can even phase separate, or "blush." This section illustrates this with experiments on a ternary system of cellulose acetate dissolved in a blend of ketone and methanol. Coatings were prepared from solutions with either acetone or methyl ethyl ketone (MEK) as the solvent, whereas the nonsolvent, methanol, remained the same in both the cases.

Experimental Studies

Commercially available cellulose acetate, with an acetyl content of 39.8 wt. % and molecular weight of 40,000 g/mol, sold as CA-398-10 grade, was obtained from Eastman Chemical Products, Inc. (Kingsport, TN). Prior to solution preparation, the polymer was vacuum-dried at 120°C for at least 12 h to remove moisture. The solvents were ACS reagent grades of acetone 99.7+%, methyl ethyl ketone 99+% (Aldrich Chemical Co., Milwaukee, WI), and methanol 99.8+% (EM Science, Gibbstown, NJ).

The phase behavior of cellulose acetate ternary solution was experimentally obtained as cloud-point data. Binary solutions of cellulose acetate in the ketones were prepared by adding the polymer, supplied in powder form, in increments. The solutions were stirred until they became visually transparent (≈ 6 h). Then, the nonsolvent, methanol, was added to these binary solutions to the point of visual onset of turbidity; the amount of nonsolvent was determined gravimetrically.

Table 3 lists the initial composition of the solutions that were used to prepare the coatings. The compositions were chosen because they had the same initial polymer weight fraction, and were located the same distance from the respective binodals. The initial solvent content could not be chosen because the two-phase region of the cellulose acetate–ketone–methanol system with MEK as the ketone is much larger than with acetone as the ketone.

Drying experiments were done by casting wet coatings with the aid of an adjustable micrometer film applicator (Paul N. Gardner Company Inc., Pompano Beach, FL) onto a Pyrex glass substrate; the wet coating was 200 μm thick, and the area of the coating was roughly 10 cm $\times$ 20 cm. Drying proceeded at ambient laboratory conditions of 22–23°C and 25–35% relative humidity.

The coatings were left in these conditions for a few hours before they were delaminated from the glass substrate with the help of a pair of tweezers. Small pieces were cut from the delaminated coatings and immersed in liquid nitrogen. The cross section was exposed by fracturing the samples by bending them with the help of a pair of tweezers. The SEM images were made with secondary electrons on a JEOL-840 SEM (Japan Electron Optics Co., Akshima, Japan). The

Table 3. Initial Compositions of Coating Solutions of Cellulose Acetate with Acetone and MEK as Ketone

Cellulose Acetate (Grade)	CA (wt. %)	Solvent (wt. %)	Nonsolvent (wt. %)
398-10	CA	Acetone	Methanol
	10	55	35
398-10	CA	MEK	Methanol
	10	75	15

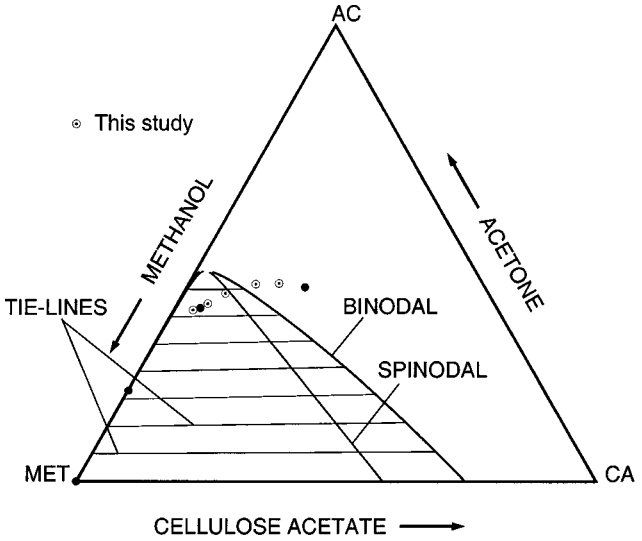

Figure 9. Phase behavior of methanol–acetone–cellulose acetate system.

● Represents data from Wagner (personal communication) (1996).

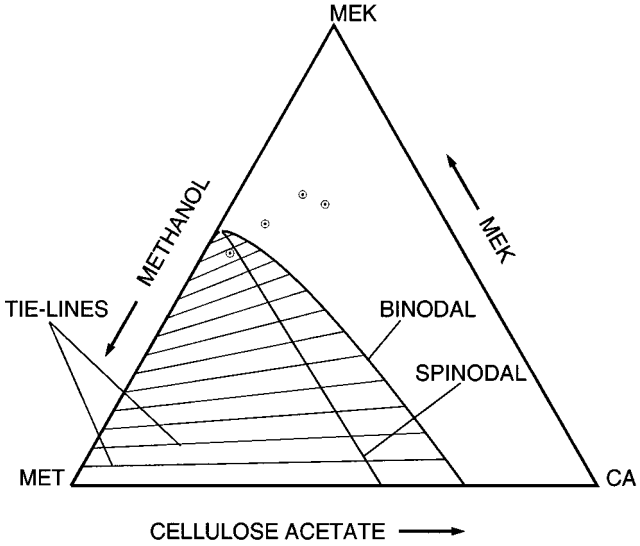

Figure 10. Phase behavior data from the methanol–MEK–cellulose acetate system.

freeze-fractured samples were mounted on a standard SEM stub with the cross section facing upwards. The samples along with the SEM stub were coated with a 5-nm-thick gold conducting layer. These samples were examined at a low 10-kV accelerating voltage.

Results

Phase diagrams

Figure 9 shows the experimental cloud-point data of the cellulose acetate–methanol–acetone system along with the predicted phase behavior from the Flory-Huggins thermodynamics of ternary polymer solutions. The predicted phase behavior is in good agreement with the experimental binodal data. Figure 10 shows the experimental cloud-point data of the cellulose acetate–MEK–methanol system. The phase boundary predicted by Flory-Huggins thermodynamics does not agree quantitatively with the cloud-point data. However, it correctly predicts a larger two-phase region when MEK replaces acetone as the solvent. The predicted binodals, in Figures 9 and 10, were obtained by using the solubility-parameter estimates.

The solubility parameter, which quantifies intermolecular forces in pure substances, can be used to predict the solubility of polymers in low molecular-weight solvents (Stoye, 1998). Three-dimensional solubility parameters take into account polymer–solvent interactions arising from dispersion forces, polar forces, and hydrogen bonding; these interactions are compounded according to the formula:

$$\delta^2 = \delta_D^2 + \delta_P^2 + \delta_H^2. \tag{2}$$

Table 4 lists the three-dimensional solubility parameters of cellulose acetate and the solvents used in this work. The Flory-Huggins binary interaction parameters are related to the solubility parameters by

$$\chi_{ij} = \frac{\overline{V}_{\text{ref}}}{RT}\left(\delta_i - \delta_j\right)^2, \tag{3}$$

where $\overline{V}_{\text{ref}}$ is the partial molar volume of the reference species, here taken as methanol.

Tables 5 and 6 list the estimated Flory-Huggins interaction parameters of the two ternary solution systems used in the experiments.

Visual observations

The wet coatings of cellulose acetate in acetone and methanol were at first visually transparent. After one minute, a turbid front began at the edges of the drying coating and proceeded inward. At 2 min after casting, the entire coating was enveloped by this turbid front. At 3 min into the drying, a bright opaque front appeared at the edges that moved inward; in another 30 s, the entire coating turned bright white. In contrast, coatings of cellulose acetate that contained MEK as the solvent remained visually transparent during the entire drying process. The next section describes the cross section of the resulting dried coatings.

Table 4. 3-D Solubility Parameters of Cellulose Acetate (Mulder et al., 1982) and Solvents (Stoye, 1998)

	$(J/cm^3)^{1/2}$			
Component	δ_D	δ_P	δ_H	δ
Cellulose acetate (CA-398)	16.16	7.2	12.9	21.9
Acetone	15.6	11.7	4.1	20.5
MEK	16.0	9.0	5.1	19.0
Methanol	15.1	11.3	22.9	29.7

Table 5. Flory-Huggins Interaction Parameters for Cellulose Acetate–Acetone–Methanol System at 25°C

Component	Molar Volume (cm^3/mol)	Interaction Parameter χ_{ij}
(1) Methanol	40.40	$\chi_{12} = 1.38$
(2) Acetone	73.32	$\chi_{23} = 0.042$
		$m_2 = 1$
(3) Cellulose acetate	30,534	$\chi_{13} = 0.942$
		$m_3 = 756$

Table 6. Flory-Huggins Interaction Parameters for Cellulose Acetate–MEK–Methanol System at 25°C

Component	Molar Volume (cm^3/mol)	Interaction Parameter χ_{ij}
(1) Methanol	40.40	$\chi_{12} = 1.87$
(2) MEK	89.44	$\chi_{23} = 0.157$
		$m_2 = 1$
(3) Cellulose acetate	30,534	$\chi_{13} = 0.942$
		$m_3 = 756$

Scanning electron microscopy images

Figure 11 shows the cross-sectional SEM image of coatings in which acetone was the solvent. It also shows the substrate side of the dried coating that was in contact with the glass substrate. The bulk of the cross-section shows pores 0.5 to 1 μm in size. The substrate side of the coating also shows the voids that form after the solvent left the polymer-lean phase.

Figure 12 shows the cross-sectional images of coatings in which the ketone used was MEK. The cross-sectional SEM images display a dense structure with no large pores. The region near the base does show some porelike features that could be due to phase separation. These pores, less than 0.3 μm large, are confined to the region near the base. This size scale of pores is small enough that they do not scatter intensely. Overall, the coating appears visually transparent because of the absence of pores at the scale of the wavelength of light.

Process-path calculations

The final microstructure of dried cellulose acetate coatings, displayed in Figures 11 and 12, can be understood by applying the process-path analysis to the drying process. The one-dimensional drying model was used to compute the process paths of cellulose acetate–ketone–methanol-based solution coatings. The solution thermodynamics, described with the Flory-Huggins theory, was used to calculate the partial pressure of solvents as a function of composition. The solvent diffusivities were estimated as their self-diffusivity in ternary polymer solutions, and were obtained from the free-volume theory of Vrentas et al. (1985):

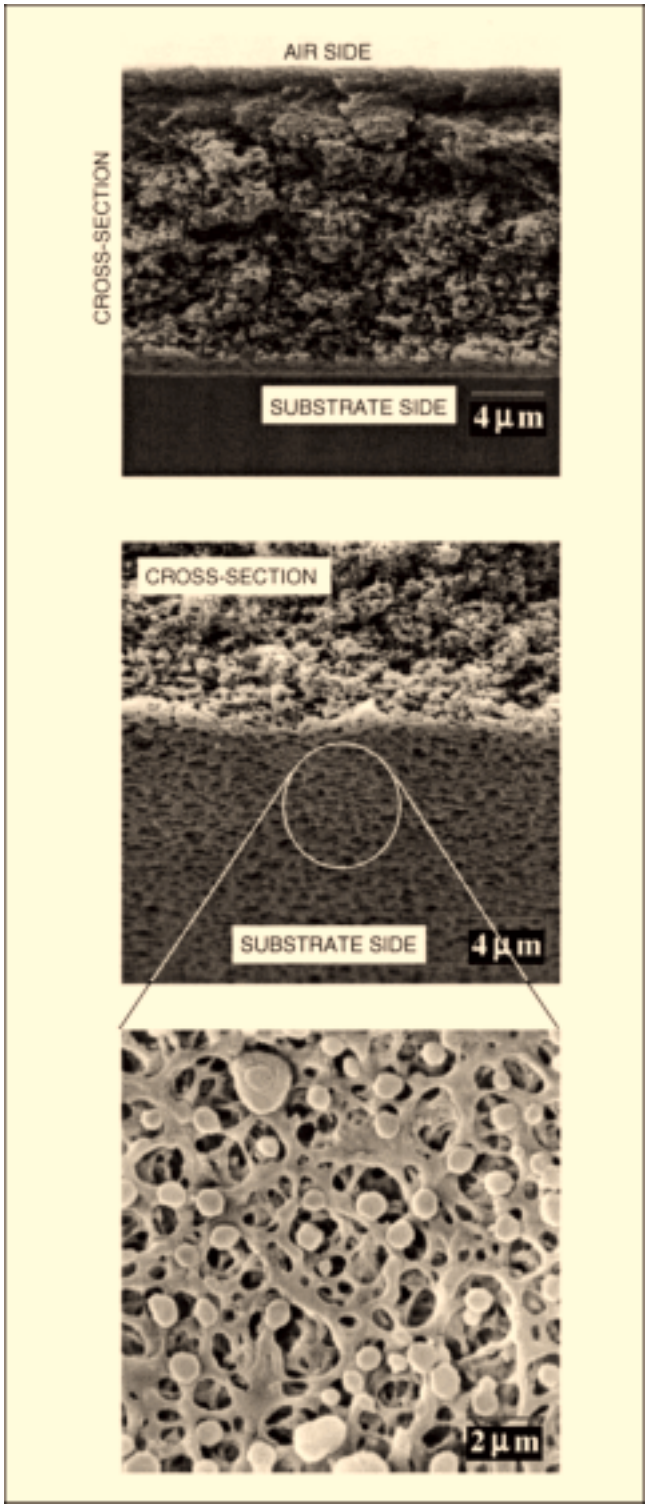

Figure 11. Cross-section of porous coatings.

$$D_1 = D_{01}\exp\left(-\frac{\phi_1\hat{V}_1^*\rho_1 + \phi_2\hat{V}_2^*\rho_2\,\xi_{13}/\xi_{23} + \phi_3\hat{V}_3^*\rho_3\,\xi_{13}}{\phi_1\dfrac{f_1}{\gamma} + \phi_2\dfrac{f_2}{\gamma} + \phi_3\dfrac{f_3}{\gamma}}\right) \tag{4}$$

$$D_2 = D_{02}\exp\left(-\frac{\phi_1\hat{V}_1^*\rho_1\,\xi_{23}/\xi_{13} + \phi_2\hat{V}_2^*\rho_2 + \phi_3\hat{V}_3^*\rho_3\,\xi_{23}}{\phi_1\dfrac{f_1}{\gamma} + \phi_2\dfrac{f_2}{\gamma} + \phi_3\dfrac{f_3}{\gamma}}\right), \tag{5}$$

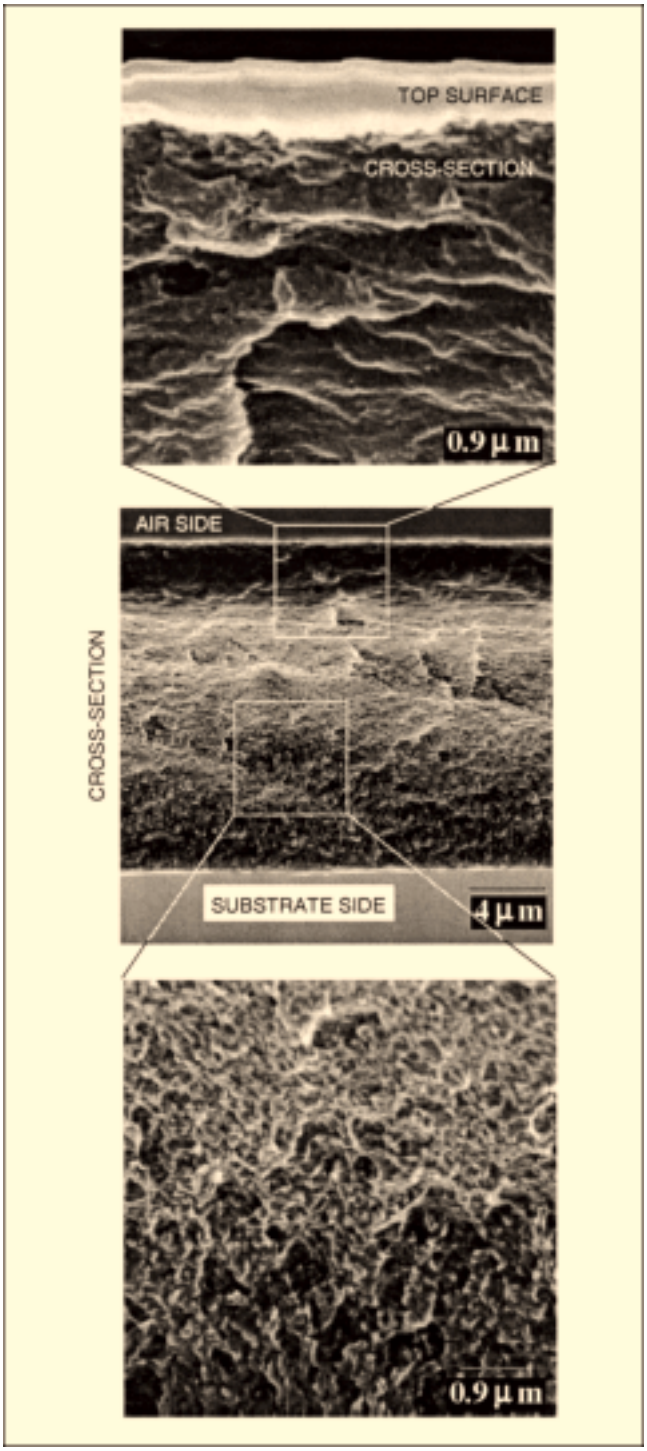

Figure 12. Cross-section of transparent coatings.

where ϕ_i and ρ_i are the volume fraction and density of the ith component. The f_i are defined as

$$\frac{f_i}{\gamma} \equiv \frac{K_{1i}}{\gamma}\left(K_{2i} + T - T_{gi}\right)\rho_i. \tag{6}$$

The binary free-volume parameters of acetone, methanol, MEK and cellulose acetate are listed in Table 7. The free-volume parameters D_{0i}, K_{1i}/γ, and $K_{2i} - T_{gi}$ are from Hong (1995). The critical volumes of solvent V_i^* were approximated as their specific volume at 0 K, $\tilde{V}_i^o(0)$, which in turn were estimated by using group contribution methods (Hong, 1995). The parameter ξ of acetone was obtained by fitting the free-volume expression of self-diffusivity of acetone to the available experimental data (Dabral, 1999). The parameter ξ of methanol and MEK were estimated by (Hong, 1995):

$$\frac{\xi_i}{\xi_{\text{acetone}}} = \frac{\tilde{V}_i^o(0)}{\tilde{V}_{\text{acetone}}^o(0)}. \tag{7}$$

Figure 13 shows the computed drying process paths of the ternary system methanol–acetone–cellulose acetate. The concentration profiles at a given time, marked in seconds, are shown by the dashed lines. In addition, the solid lines are the concentration as a function of time at a given relative depth, η. The initial mass Biot number of acetone is 6.11 and that of methanol is 1.86. This difference in magnitude is due to the higher volatility of acetone. Consequently, acetone departs rapidly during the initial stages of drying. The process paths, in turn, bend toward the methanol vertex because of faster acetone loss, causing them to invade the two-phase region. Although methanol has a higher diffusivity than acetone, the process paths near the base region do not bend toward the cellulose acetate–acetone side of the triangular composition diagram. This is because the mass Biot numbers fall in the intermediate range where neither of the resistances, diffusional and external gas phase, dominate. The resulting process paths of the bulk of the coating enter the two-phase region and likely cause phase separation, which leads to porous coatings, in agreement with the images shown in Figure 11.

When acetone is replaced by MEK, the solution evades the two-phase region because of the lower volatility and diffusivity of MEK. Figure 14 shows the process paths of the ternary system methanol–acetone–cellulose acetate. The initial Biot number of MEK is 3.07 and that of methanol is 1.86. The initial stage of drying is controlled by resistance to mass transfer in the gas phase, and the process paths of the entire coating merge into a single path, as shown in Figure 3. The resulting process paths are primarily determined by the relative volatility of the solvents. As drying proceeds and solvent content falls, the diffusivities of both methanol and MEK plummet, and the drying is controlled by diffusional resistance within the coating. Consequently, the process paths diverge toward the later stages of drying, as shown in Figure 14. The figure also shows that the entire family of process paths evades the two-phase region, so that the resulting coatings should be dense polymer films, in agreement with images of Figure 12.

Conclusion

Process-path analysis of the drying of coatings that are deposited as a polymer dissolved in mixed solvents can be illustrated with a model ternary polymer–solvent–nonsolvent system. The influence of drying process parameters, like the ex-

Table 7. Estimates of Free-Volume Parameters of Methanol, Methyl Ethyl Ketone, Acetone, and Cellulose Acetate

Property	Methanol	MEK	Acetone	Cellulose Acetate
Molec. wt., g/mol	32	72	58	40,000
Density, g/cm^3	0.7914	0.805	0.792	1.31
D_{0i}, cm^2/s	8.75×10^{-4}	16.04×10^{-4}	3.6×10^{-4}	—
$\hat{V}_i^*$, g/cm^3	0.961	0.997	0.943	1
K_{1i}/γ, cm^3/(g·K)	1.17×10^{-3}	0.73×10^{-3}	1.86×10^{-3}	4.82×10^{-4}
$K_{2i}-T_{gi}$, K	−48.41	59.63	−53.33	−180
ξ_{i3}	0.5814	1.353	1.08	—

Source: Data from Hong (1995).

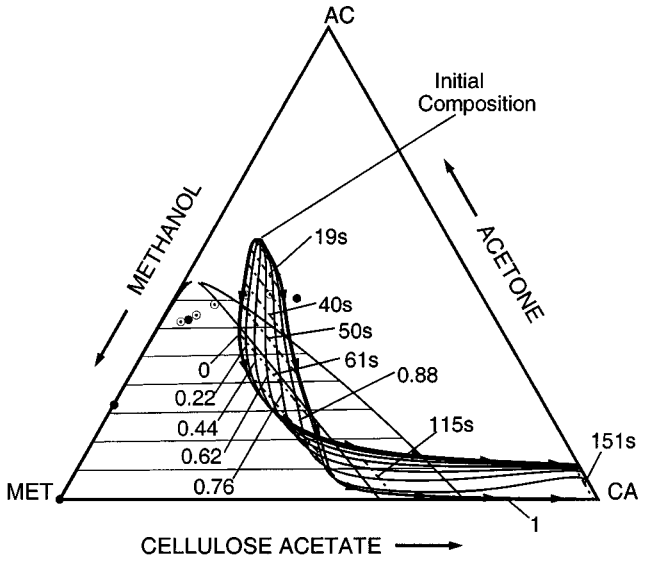

Figure 13. Drying-process paths of ternary cellulose acetate solutions with acetone as the ketone.

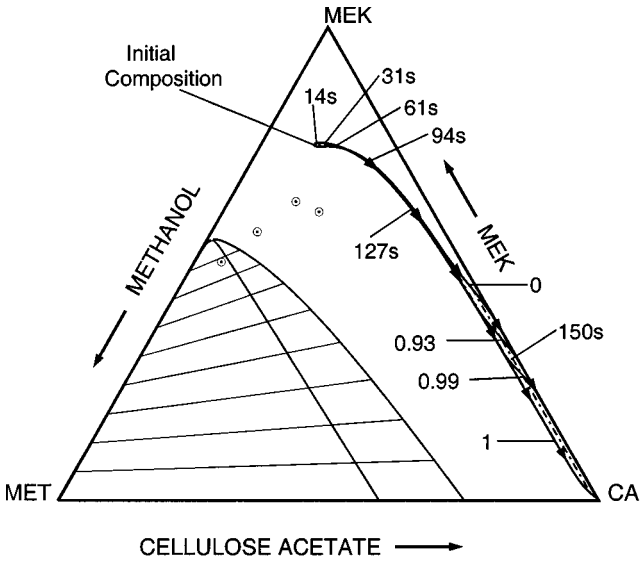

Figure 14. Drying-process paths of ternary cellulose acetate solutions with MEK as the ketone.

ternal gas-phase mass-transfer coefficient, partial pressures of solvents in the adjoining phase, and solvent relative volatility and diffusivity, are made clear. During drying, the process paths may invade thermodynamically-unstable regions or may pass through regions of vitrification, gelation, and/or crystallization. The distribution of local states with depth, isochronals, or "time lines," are thus crucial in determining the state of the solution coating. Passing into or through the two-phase region can lead to spinodal decomposition or nucleation and growth. If phase separation is to be avoided, one possibility is to choose solvents with low volatility and diffusivity, but doing so lengthens drying time. Another possibility is to control the relative drying rates of "solvent" and "nonsolvent," by adjusting the partial pressure of volatiles in the gas phase; however, doing this may lengthen drying time, too, unless other process conditions can be changed. The invasion of the isochronals into the solidification region is an equally important variable in cases where solidification by drying induces or competes with other rate processes, like phase separation, crystallization, or gelation. Gradients in time to solidify along the process paths can set up gradients in microstructure. These may be desirable or undesirable, depending on the requirements of the final microstructure of the coating. In sum, process-path analysis of drying coatings serves as a process design tool and can guide in controlling the drying conditions to achieve a desirable microstructure.

Acknowledgments

This research was funded by sponsors of the Coating Process Fundamentals Program of the Center for Interfacial Engineering. Dr. James R. Wagner of Imation provided experimental data and examples of blush in solvent cast coatings. Zhisong Huang helped in obtaining the SEM images of the final samples.

Notation

D_0 = reference diffusion coefficient
L_0 = initial film thickness
t = time
z = position from the base of the coating
α = relative volatility
α_1 = initial nonsolvent volume fraction

Literature Cited

Adachi, A., and L. E. Scriven, "Solute Migration During Drying (Isothermal Case Study)," *Int. Symp. on Coating Science and Technology*, AIChE Meeting, New Orleans, LA (1992).
Cairncross, R. A., L. F. Francis, and L. E. Scriven, "Competing Drying and Reaction Mechanisms in the Formation of Sol-to-Gel Films, Fibers and Spheres," *Drying Technol. J.*, **10**, 893 (1992).

Cheng, L. P., Y. S. Soh, A. H. Dwan, and C. C. Gryte, "An Improved Model for Mass Transfer During the Formation of Polymeric Membranes by the Immersion-Precipitation Process," *J. Poly. Sci. Part B: Poly. Phys.*, **32**, 1413 (1994).

Dabral, M., "Solidification of Coatings: Theory and Modeling of Drying, Curing and Microstructure Growth," PhD Thesis, Univ. of Minnesota, Minneapolis (1999).

Flory, P. J., *Principles of Polymer Chemistry*, Cornell Univ. Press, Ithaca, NY (1953).

Hong, S. U., "Prediction of Polymer/Solvent Diffusion Behavior Using Free Volume Theory," *J. Poly. Sci. Part B: Poly. Phys.*, **34**, 2536 (1995).

Kesting, R. E., *Synthetic Polymeric Membranes: A Structural Perspective*, Wiley, New York (1985).

Koros, W. J., and I. Pinnau, "Membrane Formation for Gas Separation Membranes," *Polymeric Gas Separation Membranes*, D. R. Paul and Y. P. Yampol'skii, eds., CRC Press, Boca Raton, FL (1994).

Mulder, M., *Basic Principles of Membranes Technology*, Kluwer, Boston (1991).

Mulder, M. H., F. Kruitz, and C. A. Smolders, "Separation of Isomeric Xylenes by Pervaporation Through Cellulose Ester Membranes," *J. Memb. Sci.*, **11**, 349 (1982).

Okazaki, M., K. Shioda, K. Masuda, and R. Toei, "Drying Mechanisms of Coated Film of Polymer Solution," *J. Chem. Eng. Jpn.*, **7**, 99 (1974).

Radovanovic, P., S. W. Thiel, and S. T. Hwang, "Formation of Asymmetric Polysulfone Membranes by Immersion Precipitation: I. Modeling Mass Transport During Gelation," *J. Memb. Sci.*, **65**, 213 (1992).

Reuvers, A. J., J. W. A. van den Berg, and C. A. Smolders, "Formation of Membranes by Means of Immersion Precipitation: A Model to Describe Mass Transfer During Immersion Precipitation," *J. Memb. Sci.*, **34**, 67 (1987).

Shojaie, S. S., W. B. Krantz, and A. R. Greenberg, "Dense Polymer Film and Membrane Formation Via the Dry-Cast Process: II. Model Validation and Morphological Studies," *J. Memb. Sci.*, **94**, 281 (1994a).

Shojaie, S. S., W. B. Krantz, and A. R. Greenberg, "Dense Polymer Film and Membrane Formation Via the Dry-Cast Process. Part I. Model Development," *J. Memb. Sci.*, **94**, 255 (1994b).

Stoye, D., "Solvents," *Paints, Coatings and Solvents*, D. Stoye and W. Freitag, eds., Wiley-VCH, New York (1998).

Strathmann, H., P. Scheible, and R. W. Baker, "A Rationale for the Preparation of Loeb-Sourirajan-Type Cellulose Acetate Membrane," *J. Appl. Poly. Sci.*, **15**, 811 (1971).

Tsay, C. S., and A. J. McHugh, "Mass Transfer Modeling of Asymmetric Membrane Formation by Phase Inversion," *J. Poly. Sci. Part B: Poly. Phys.*, **28**, 1327 (1990).

Tsujimoto, T., "Solution Film Casting Technology," *Proc. Int. Coating Science and Technology Symp.*, Int. Soc. of Coating Sci. and Technol. Newark, DE (1998).

Vrentas, J. S., and J. L. Duda, "Diffusion," *Encyclopedia of Polymer Science and Engineering*, Vol. 5, 2nd ed., Wiley, New York (1987).

Vrentas, J. S., J. L. Duda, and H. C. Ling, "Enhancement of Impurity Removal from Polymer Films," *J. Appl. Poly. Sci.*, **30**, 4499 (1985).

Vrentas, J. S., and C. M. Vrentas, "Drying of Solvent Coated Polymer Films," *J. Poly. Sci. Part B: Poly. Phys.*, **32**, 187 (1994).

Wagner, J., "Cloud Point Measurements of Cellulose Acetate Dissolved in Acetone and Methanol," personal communication, unpublished results (1996).

Yilmaz, L., and A. J. McHugh, "Analysis of Nonsolvent-Solvent-Polymer Phase Diagram and Their Relevance to Membrane Formation Modeling," *J. Appl. Poly. Sci.*, **31**, 997 (1986).

Manuscript received Dec. 2, 1999, and revision received June 11, 2001.